J Therm Spray Tech (2017) 26:140–149
DOI 10.1007/s11666-016-0486-5

PEER REVIEWED

Hot Corrosion Mechanism in Multi-Layer Suspension Plasma Sprayed $Gd_2Zr_2O_7$ /YSZ Thermal Barrier Coatings in the Presence of V_2O_5 + Na_2SO_4

Krishna Praveen Jonnalagadda[1] · Satyapal Mahade[2] · Nicholas Curry[3] · Xin-Hai Li[4] · Nicolaie Markocsan[2] · Per Nylén[2] · Stefan Björklund[2] · Ru Lin Peng[1]

Submitted: 30 May 2016 / in revised form: 15 August 2016 / Published online: 7 December 2016

Abstract This study investigates the corrosion resistance of two-layer $Gd_2Zr_2O_7$/YSZ, three-layer dense $Gd_2Zr_2O_7$/$Gd_2Zr_2O_7$/YSZ, and a reference single-layer YSZ coating with a similar overall top coat thickness of 300-320 µm. All the coatings were manufactured by suspension plasma spraying resulting in a columnar structure except for the dense layer. Corrosion tests were conducted at 900 °C for 8 h using V_2O_5 and Na_2SO_4 as corrosive salts at a concentration of approximately 4 mg/cm^2. SEM investigations after the corrosion tests show that $Gd_2Zr_2O_7$-based coatings exhibited lower reactivity with the corrosive salts and the formation of gadolinium vanadate ($GdVO_4$), accompanied by the phase transformation of zirconia was observed. It is believed that the $GdVO_4$ formation between the columns reduced the strain tolerance of the coating and also due to the fact that $Gd_2Zr_2O_7$ has a lower fracture toughness value made it more susceptible to corrosion-induced damage. Furthermore, the presence of a relatively dense layer of $Gd_2Zr_2O_7$ on the top did not improve in reducing the corrosion-induced damage. For the reference YSZ coating, the observed corrosion-induced damage was lower probably due to combination of more limited salt penetration, the SPS microstructure and superior fracture toughness of YSZ.

Keywords gadolinium zirconate · hot corrosion · multi-layer thermal barrier coatings · suspension plasma spraying · vanadium pentoxide + sodium sulfate

Introduction

Thermal barrier coatings (TBCs) are widely employed in gas turbines for protecting components operating at high temperatures (Ref 1-5). TBCs are advanced material systems comprising of at least two layers; first layer is a metallic bond coat of MCrAlY type where M represents either Ni/Co or both, Cr and Al for chromium and aluminum respectively, Y is a minor reactive element yttria and the second layer being a ceramic top coat. These coatings are typically deposited by thermal spraying technique using powder as the raw feed stock. TBCs, when exposed to the harsh conditions in the gas turbine, regularly suffer from oxidation and/or corrosion.

Yttria-stabilized zirconia (YSZ) with 7-8 wt.% yttria is currently the industrial standard for the top coat material. YSZ has several attractive properties such as low thermal conductivity, high fracture toughness, and high coefficient of thermal expansion and therefore has been used as top coat material for many decades. One of the limitations with YSZ is the high-temperature operating limit of 1200 °C above which the phase stability of zirconia becomes an issue. Exposure at or above 1200 °C for longer time leads

This article is an invited paper selected from presentations at the 2016 International Thermal Spray Conference, held May 10-12, 2016, in Shanghai, P.R. China, and has been expanded from the original presentation.

✉ Krishna Praveen Jonnalagadda
Praveen.jonnalagadda@liu.se

[1] Department of Management and Engineering, Linköping University, 581 83 Linköping, Sweden

[2] Department of Engineering Science, University West, Trollhättan, Sweden

[3] Treibacher Industrie AG, Althofen, Austria

[4] Siemens Industrial Turbomachinery AB, 61283 Finspång, Sweden

to transformation of tetragonal prime (t') to yttria-rich cubic (c) and yttria-poor tetragonal zirconia. Tetragonal zirconia is not stable at the operating temperatures of gas turbine, and during cooling it transforms to monoclinic zirconia. This results in a volume expansion of 3-5% that is sufficient to induce cracking and damage in the coating (Ref 6). In addition, YSZ is prone to corrosive attack from species such as vanadium and sulfur which causes accelerated phase transformation of zirconia from t' to monoclinic (Ref 7, 8). The source for these corrosive species is from the low-grade fuel used in industrial gas turbines.

With demands now on more efficient gas turbines, there is an active search for new TBC materials that could replace the conventional YSZ (Ref 9, 10). Among the new materials, gadolinium zirconate (GZ) appears promising with low thermal conductivity and high-temperature phase stability compared to YSZ. One of the limitations with gadolinium zirconate is that it is not thermodynamically compatible with alumina, the thermally grown oxide that grows at the interface between the metallic bond coat and the ceramic top coat. It forms a porous layer of $GdAlO_3$ thereby reducing the resistance of the coating to oxidation (Ref 11). It is therefore deposited over the top of YSZ forming a multi-layer coating system. Studies on the corrosion resistance of atmospheric plasma sprayed (APS) gadolinium zirconate with vanadium pentoxide and sodium sulfate show that gadolinium zirconate has better corrosion resistance compared to YSZ (Ref 8).

In addition to the TBC material, coating deposition techniques can have significant impact on the overall lifetime of TBCs. A new emerging technique, suspension plasma spraying (SPS), is known to produce columnar structures. It is believed that SPS deposited coatings exhibit better cyclic life compared to the conventional APS coatings where the microstructure is a typical splat on splat structure (Ref 12-14). The right combination of TBC material and the deposition process can result in more durable coating and improve the lifetime of the coatings. Also, the new materials and processes developed should outperform conventional YSZ if they are to be considered as a potential replacement. Previous research on gadolinium zirconate's corrosion resistance has been focused on only APS deposited coatings. To the best of authors' knowledge, no work has been done on the corrosion resistance of SPS deposited gadolinium zirconate TBCs. In this work, a two-layer gadolinium zirconate/YSZ and a three-layer dense gadolinium zirconate/gadolinium zirconate/YSZ TBCs were deposited by SPS, and their hot corrosion behavior in the presence of vanadium pentoxide (V_2O_5) and sodium sulfate (Na_2SO_4) has been studied. A reference coating of 8 wt.% YSZ has also been included for comparison.

Experiment

Materials

The TBC systems studied in this work consisted of Hastelloy X substrate (Ni22Cr1.5Co0.5W9Mo18Fe1Si). The top surface is a rectangular shaped bar, 50 × 30 mm and 5 mm in thickness, which was grit blasted using alumina particles of 220 grit size, and a surface roughness (R_a) of 3 μm was obtained. On the top of the grit blasted substrates, a metallic bond coat was deposited using the High Velocity Air Fuel (HVAF) system to obtain a nominal thickness of 220 μm. The bond coat material used was AMDRY 9951 (Co32Ni17Cr8Al0.5Y). Grit blasting of the bond coat substrate was carried out using alumina particles in order to remove the oxides present on the surface.

Suspension Plasma Spray Setup and Spray Parameters for the Top Coat

The top coat in the three TBC systems was deposited by suspension plasma spray process using the Axial III plasma gun (Northwest Mettech Corp, Vancouver, Canada) and Nanofeed 350 suspension feeding system. The suspension plasma spray setup comprises of a liquid feedstock vessel to hold the suspension. The vessel also has a mechanical stirrer which operates throughout the process to ensure that the suspension remains fully dispersed. Suspension (feedstock) is then pumped to the plasma torch using a peristaltic pump. Feedstock flow is controlled by a coriolis flow meter. During the spray process, the suspension and atomizing gas are coaxially fed into the Mettech Axial III plasma gun. The gun accommodates three plasma exit ports which direct the plasma to converge at their geometric center. The liquid feedstock meets the converging plasma axially. An additional nozzle is present at the end of plasma gun to further narrow down the exiting plasma directed onto the rotating fixture. Further details of the spray process are discussed in our previous work (Ref 14).

For this work, two different ethanol-based suspensions were produced by Treibacher Industrie AG (Althofen, Austria). The materials were YSZ and gadolinium zirconate. Both suspensions had a median particle size of 500 nm and a solids load of 25% weight in ethanol solvent. Two different spray parameters were employed for depositing the single-, double-, and triple-layer TBCs, as shown in Table 1. The first parameter was optimized to create a columnar microstructure, whereas the second parameter was chosen to deposit a relatively dense gadolinium zirconate (GZ) layer. All the top coat systems were deposited to achieve an overall thickness of 300-320 μm. The TBC samples were later cut at the center

using water-jet cutting to produce samples of size 25 × 30 mm. The coating architecture is shown in Fig. 1.

Corrosion Tests

Corrosion tests were conducted using a mixture of vanadium pentoxide (V_2O_5) and sodium sulfate (Na_2SO_4) in the ratio of 55:45 wt.%. The salts were manually mixed and spread over the coating surface to get a concentration of approximately 4 mg/cm^2 (salt concentration selected was based on earlier unpublished corrosion tests on APS coatings). The samples were later placed in the furnace already heated to 900 °C. The samples were held at that temperature for 8 h after which they were removed and allowed to cool in air.

Characterization

The corroded samples were subjected to XRD (Pan Analytical X'pert Pro) for phase analysis. After XRD, the samples were investigated in the SEM for observing the top surface and the cross sections using energy-dispersive x-ray Spectroscopy (EDS). In addition, porosity analysis was done on the as-sprayed samples using ImageJ (available in public domain). For the image analysis, twenty-five different SEM micrographs at 500× magnification were considered to analyze the porosity content of the as-sprayed TBCs. A magnification of 500× was chosen for two reasons: The first one is that this magnification is high enough to take into account of the porosity contribution due to columnar gaps and fine scale porosity in the TBC. The second reason is that it gave good contrast between the ceramic and the pores in the TBCs. The average porosity value in each coating system is shown in Fig. 2.

Table 1 Spray parameters

Parameters	Columnar layer	Dense layer
Standoff distance (mm)	75	70
Median particle size of solute (D_{50}) in nm	500	500
Atomizing gas flow (l/min)	20	5
Jet Enthalpy (kJ)	7	11
Power (kW)	89	103
Total gas flow (l/min)	245	200

Results and Discussions

As-sprayed Microstructures

Figure 3(a)-(c) show the cross sections of as-sprayed single-layer YSZ, double-layer gadolinium zirconate (GZ)/YSZ, and the three-layer dense gadolinium zirconate (DGZ)/GZ/YSZ, respectively. In all the three coating systems, good interface between the different top coat layers (without pores or cracks) was observed. Columns and columnar boundaries formed during the deposition process can be observed in the coatings. The third layer of the coating (Fig. 3c) has a relatively dense and compact structure and not a columnar one. It is believed that having a compact structure can delay the infiltration of the molten corrosive salts compared to a columnar structure.

Top View of the Coatings: Before and After Corrosion

Figure 4(a)-(c) shows the top surface of the coatings before corrosion. The dark area in the pictures represents the gaps between the columns. Figure 4(d)-(f) shows the top surface after corrosion. These pictures were taken in the region where there was no spallation to determine the extent of corrosive product formation. Corrosive products YVO_4 (for the YSZ coating) and $GdVO_4$ (for the $Gd_2Zr_2O_7$ coating) were observed. Figure 5 shows the EDS maps confirming that the corrosive product formed in the gadolinium zirconate coating is $GdVO_4$. Due to the relatively dense structure in the top layer in three-layer coating system, the corrosive salts may not penetrate much into the surface and hence $GdVO_4$ appears to be clustered (Fig. 4f).

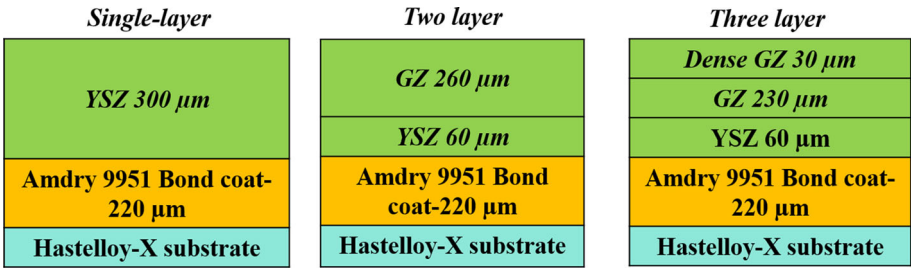

Fig. 1 Different coating architectures

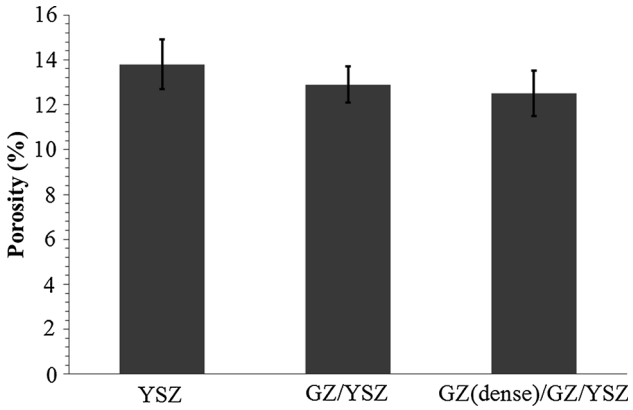

Fig. 2 Porosity analysis showing average porosity value in each coating system

XRD Results: Before and After Corrosion

The top surface of as-sprayed TBCs was analyzed using XRD for their phase composition and is shown in Fig. 6(a). The peaks obtained by XRD measurements were labeled using JCPDS standard. In the single-layer 8 wt.% YSZ TBC, the tetragonal prime phase of zirconia was observed. This phase is beneficial for the longer durability of TBC when exposed to thermal cyclic conditions as it remains stable up to 1200 °C. However, in the case of GZ-based multi-layered TBCs, a cubic defect fluorite phase of gadolinium zirconate was obtained. The defect fluorite phase is a disordered variation of the cubic pyrochlore structure where the cations and oxygen vacancies occupy random positions in the cubic crystal structure (Ref 15). This cubic phase of gadolinium zirconate is stable up to its melting temperature range which is highly desirable for TBC applications.

XRD analysis on the top surface of the corroded TBCs is shown in Fig. 6(b). For gadolinium zirconate-based coatings (both two layer and three layer), $GdVO_4$ was observed along with monoclinic zirconia. The reaction between the corrosive salts and gadolinium zirconate is believed to be either of (1) or (2). Na_2SO_4 does not react directly with $Gd_2Zr_2O_7$ (Ref 16). However, it reacts with V_2O_5 to form sodium metavanadate ($NaVO_3$), with a melting point of 610 °C, as shown in (3). Also, Na_2O can react directly with V_2O_5 forming $NaVO_3$ as shown in (4). For the single-layer YSZ coating, YVO_4 along with monoclinic zirconia was observed which agree well with the EDS maps. Also, a qualitative comparison on the volume fraction of m-ZrO_2 was made based on the intensity values for the three coatings as the same set up during XRD has been used.

$$Gd_2Zr_2O_7 + 2NaVO_3(l) \rightarrow 2GdVO_4 + \text{m-}2ZrO_2 + 2Na_2O(l) \quad \text{(Eq 1)}$$

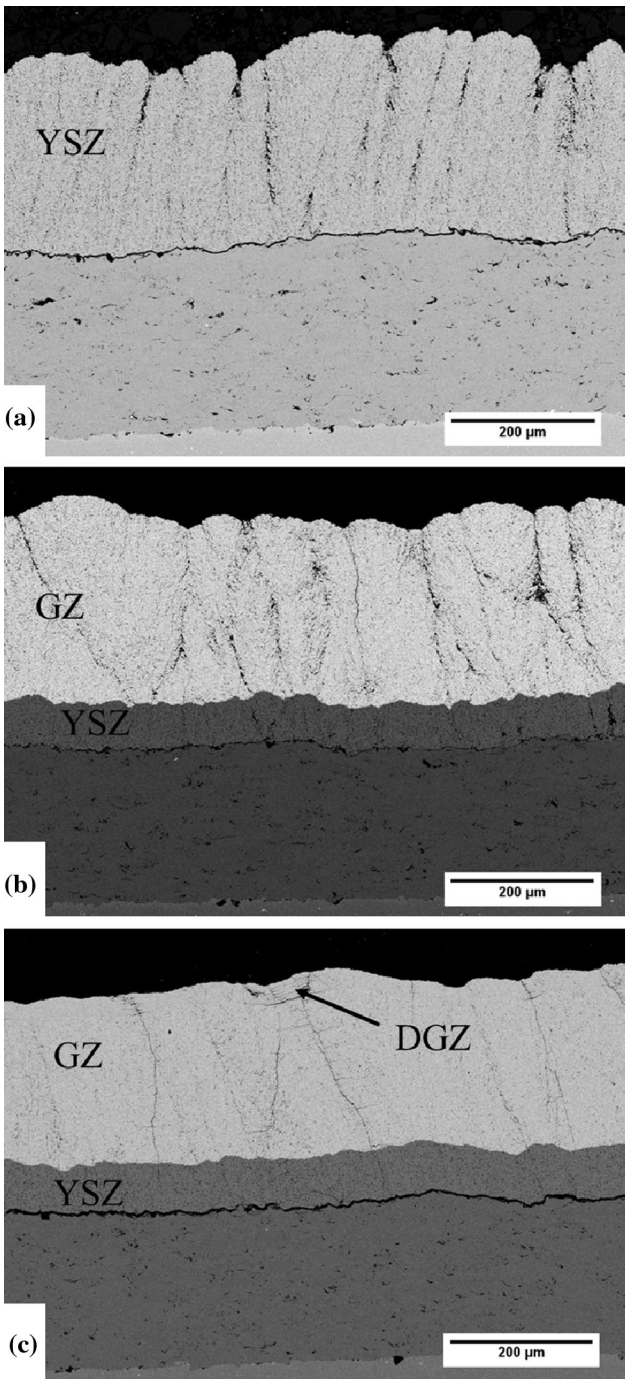

Fig. 3 Showing as-sprayed microstructures of (a) YSZ, (b) GZ/YSZ, and (c) DGZ/GZ/YSZ

$$Gd_2Zr_2O_7 + V_2O_5 \rightarrow 2GdVO_4 + \text{m-}ZrO_2 \quad \text{(Eq 2)}$$

$$Na_2SO_4 + V_2O_5 \rightarrow 2NaVO_3 + SO_3(g) \quad \text{(Eq 3)}$$

$$Na_2O(l) + V_2O_5(l) \rightarrow 2NaVO_3(l) \quad \text{(Eq 4)}$$

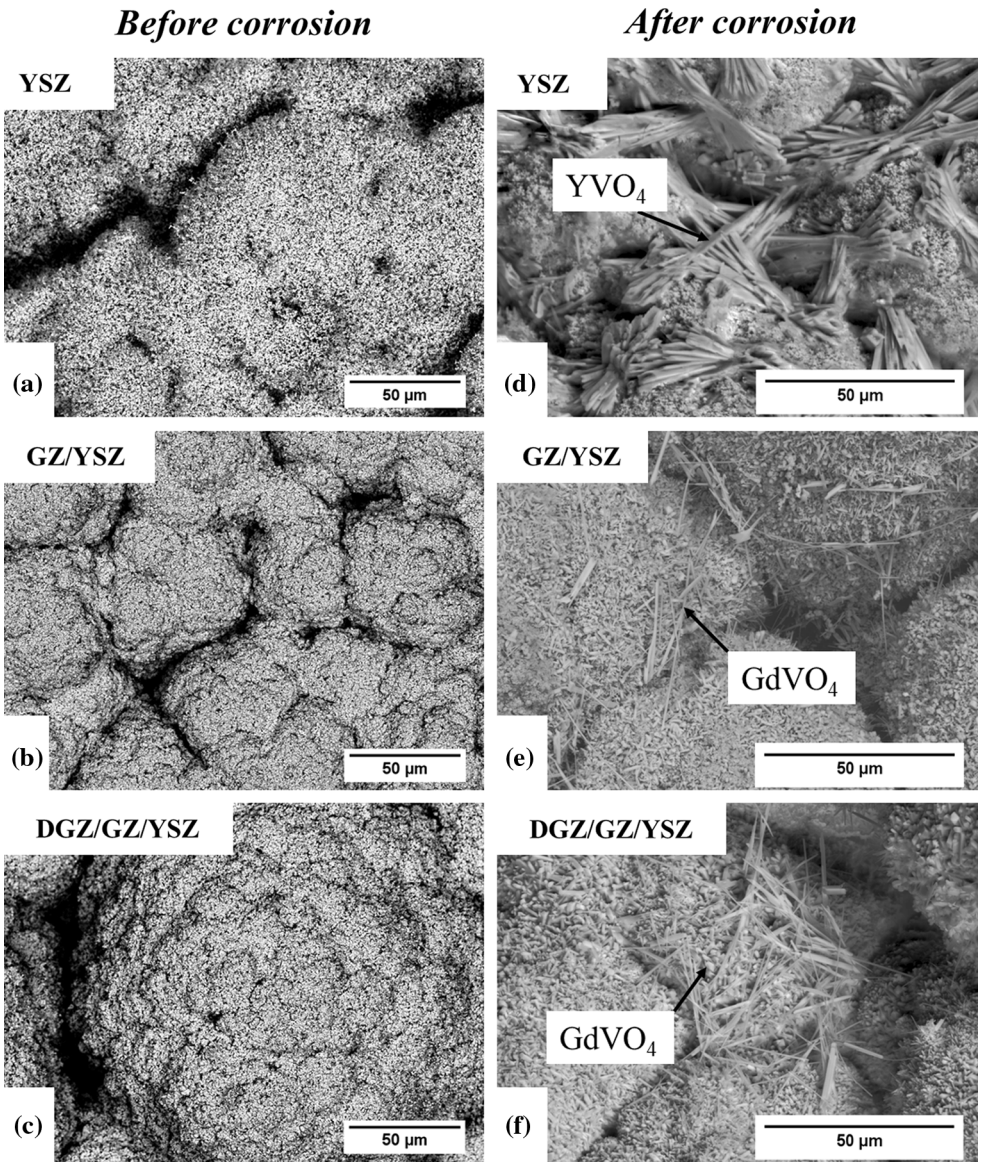

Fig. 4 Top view of the coatings (a-c) before corrosion of YSZ, GZ/YSZ and DGZ/GZ/YSZ, and (d-f) after corrosion of the coatings shown in (a-c), respectively

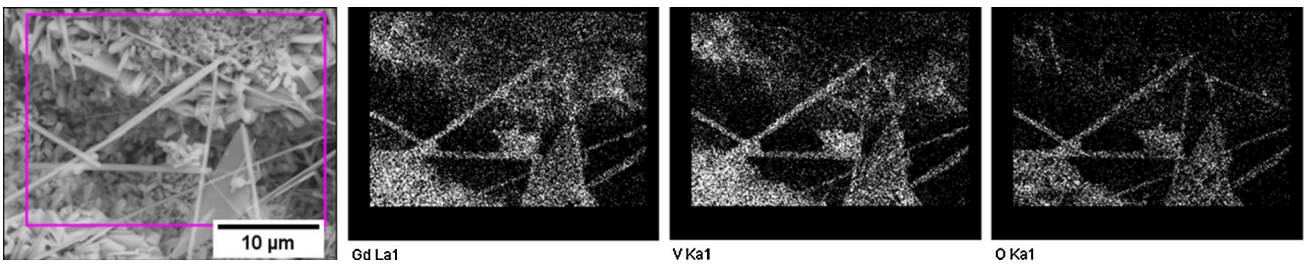

Fig. 5 EDS maps of the top corroded surface in $Gd_2Zr_2O_7$ coating system

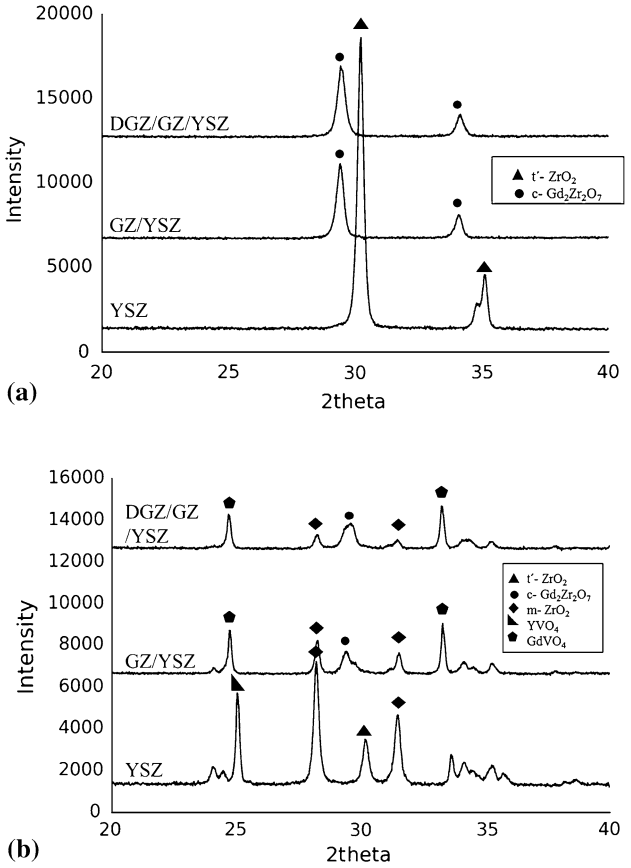

Fig. 6 X-ray diffration pattern on the top coat surface (a) before and (b) after corrosion tests

Cross Section and Corrosion Mechanism of SPS YSZ

Figure 7(a) shows the cross section of the corroded SPS YSZ sample. The corrosive salts at the exposure temperature melt and infiltrate the coating. The columnar gaps in the SPS coating act as effective path ways for the molten salts. Corrosive salts, once inside the columnar gaps, enter the pores to the sides and fill them. These salts react with the zirconia stabilizer, yttria, and form YVO_4 (Fig. 7b) thereby leaching yttria from the YSZ coating. Figure 7(c) shows the formation of YVO_4 in the coating with EDS maps and this results in transformation of zirconia from tetragonal prime to monoclinic with a 3-5% volume change sufficient to damage the coating. In addition, compressive growth stresses due to YVO_4 formation also contribute to the damage. The net result of these two types of stresses leads to crack formation in the coating (in these case horizontal cracks as shown from Fig. 7a). The presence of horizontal cracks is assumed to be due to the stress differences in X and Y directions as observed by Abubakar et al. (Ref 17). However, the extent of columnar microstructure effect on the horizontal cracks is unclear at present and is subject of future research. It has to be noted that the horizontal cracks present did not result in spallation of the coating within the testing time of the current experiment.

Cross Section and Corrosion Mechanism of SPS GZ and SPS DGZ

Like with the single-layer YSZ coating, the columnar gaps act as effective pathways for the molten salts to infiltrate. The infiltrated salts react with gadolinium zirconate and form $GdVO_4$, resulting in the phase transformation of zirconia similar to the case with YSZ. However, unlike YSZ, gadolinium zirconate has lower reactivity with the corrosive salts. This is because the corrosion reaction follows Lewis acid-base mechanism where the compound with higher basicity has higher tendency to react with the compound with stronger acidity. As reported in the literature, basicity of gadolinia (Gd_2O_3) is lower than yttria (Y_2O_3) (Ref 8). This will result in the lower reactivity for gadolinia compared to yttria with the corrosive salts. Due to the lower reactivity, the molten salts do not enter the pores as much as in YSZ but rather stay at the columnar gaps. This results in the formation of a layer of $GdVO_4$ on the top surface and in between the columns as shown in Fig. 8(a) and (b). Figure 8(c) and (d) shows the qualitative and the quantitative EDS maps of the corroded layer formed between the columns. Figure 8(e) shows the horizontal cracks in the gadolinium zirconate layer, and Fig. 8(f) shows partial spallation of the second layer in the coating.

Figure 9(a) and (b) shows the cracks in both the second and third layer of a three-layer coating system respectively. In this coating system, spallation had occurred in the second layer similar to the two-layer system (not shown in the figures). The molten salts initially react with the compact layer of $Gd_2Zr_2O_7$ forming $GdVO_4$. The stresses in this case may not be relieved as the layer is relatively dense and causes cracks in the third layer and close to the interface between the third and the second layer (Fig. 9b). Moreover, due to the presence of vertical cracks in the third layer (Fig. 9a), the salts infiltrate through them and cause damage from inside the coating (the second layer).

Discussion

From the results of corrosion tests, more specifically from Fig. 4(d)-(f), the volume fraction of $GdVO_4$ is significantly lower, compared to YSZ, as seen from the top surface of the corroded samples. In the beginning, following the nucleation and the growth mechanism, both YVO_4 and

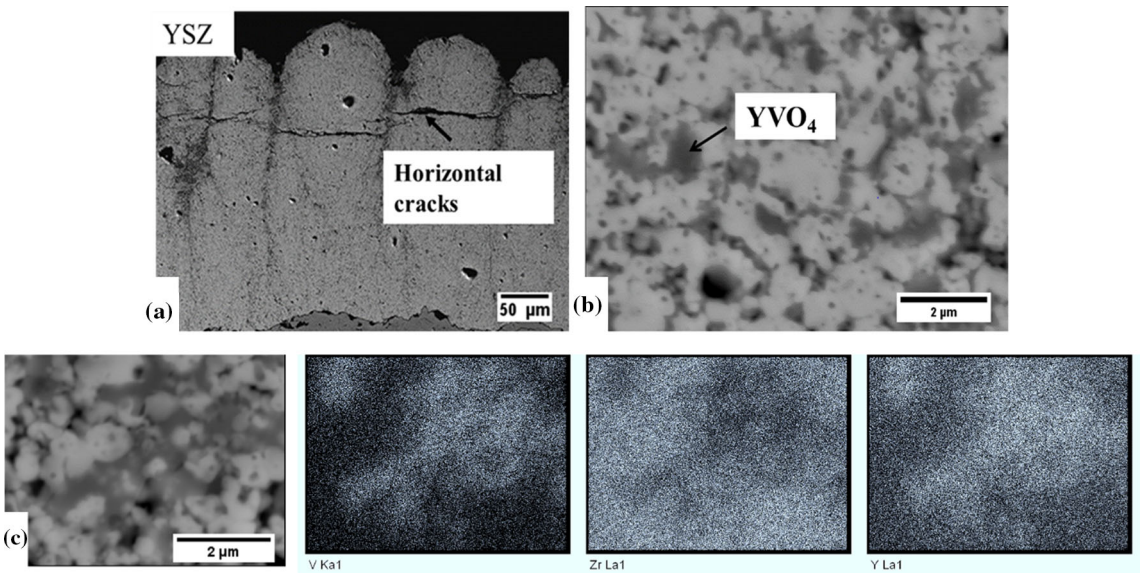

Fig. 7 Cross section of YSZ showing (a) horizontal cracks (b) YVO_4 formation, and (c) EDS map of the corrosive product

$GdVO_4$ have dendritic structures but as with increased exposure time YVO_4 dendrites change to more rod-like shape. $GdVO_4$ is thermodynamically more stable than YVO_4 which helps $GdVO_4$ retain its thinner dendritic like appearance (Ref 8). Also as mentioned above, corrosion mechanism is similar in both the materials with the main difference being the lower reactivity for gadolinia. This may provide gadolinium zirconate a better corrosion resistance (Ref 8).

In the results presented here, from Fig. 7(a) and 8(e), the cracks in the YSZ coating are present in the upper part of the coating, while for GZ coating cracks were observed through the coating thickness. As the YSZ coating is more reactive with the corrosive salts, the salts tend to become immobilized within the upper part of the coating structure. For GZ coating, due to the low reactivity of the salts and columnar microstructure, deeper infiltration of salts occurs, and therefore, corrosive products are observed through the thickness of the coating. This may explain the reason for the presence of cracks in the GZ coating through the coating thickness.

To understand why the crack lengths (no the location of the cracks) are larger in GZ coating compared to YSZ coating, it has to be looked in the context of the microstructure and material combination. An SPS coating with a columnar structure (similar to an EB-PVD coating) gets its strain tolerance from the loosely bonded columns. The inter-column gaps have near zero elastic modulus. Strain within the coating is accommodated by free expansion (or contraction) of the columns into the gaps, which should result in negligible stress build-up in the coating (Ref 18). The above argument while true for thermal stresses caused due to the substrate/TC CTE mismatch may also be possibly extended to the case of zirconia phase transformation. When the phase transformation is considered in a single column, it could result in stress and cracking as the column itself has limited ability to relieve such stress. However, at the column edge, the structure should be free to expand to accommodate the stress. The authors' assume that this could result in stress relief to certain extent. Furthermore, for an SPS coating with a columnar microstructure, crack propagation may not be easy through the coating cross section due to the columnar gaps. However, if the formation of the corrosive salts seal up the columnar structure, as in the case of gadolinium zirconate-based coatings, then first the strain tolerance of the coatings is reduced; second the cracks can propagate much more easily throughout the coating due to the loss of columnar structure. As a consequence of this gadolinium zirconate-based coatings showed large cracks and at some locations even spallation. The corrosion-induced damage process can also depend on the porosity of the coating, which depends on the deposition process. From Fig. 2, the average porosity value in all the coatings is similar, and thus, the effect of porosity on corrosion-induced damage for GZ and YSZ can be assumed to be negligible.

An important factor that effects how easily the cracks can propagate through the coating is its fracture toughness. From the literature, the fracture toughness value for GZ is about 1 MPa $m^{1/2}$, while that of YSZ is about 2 MPa $m^{1/2}$ or higher as reported by various researchers (Ref 19, 20). As the fracture toughness of GZ is lower than YSZ, cracks formed in the gadolinium zirconate layer are expected to propagate easily. In addition, when YVO_4 and $GdVO_4$ are

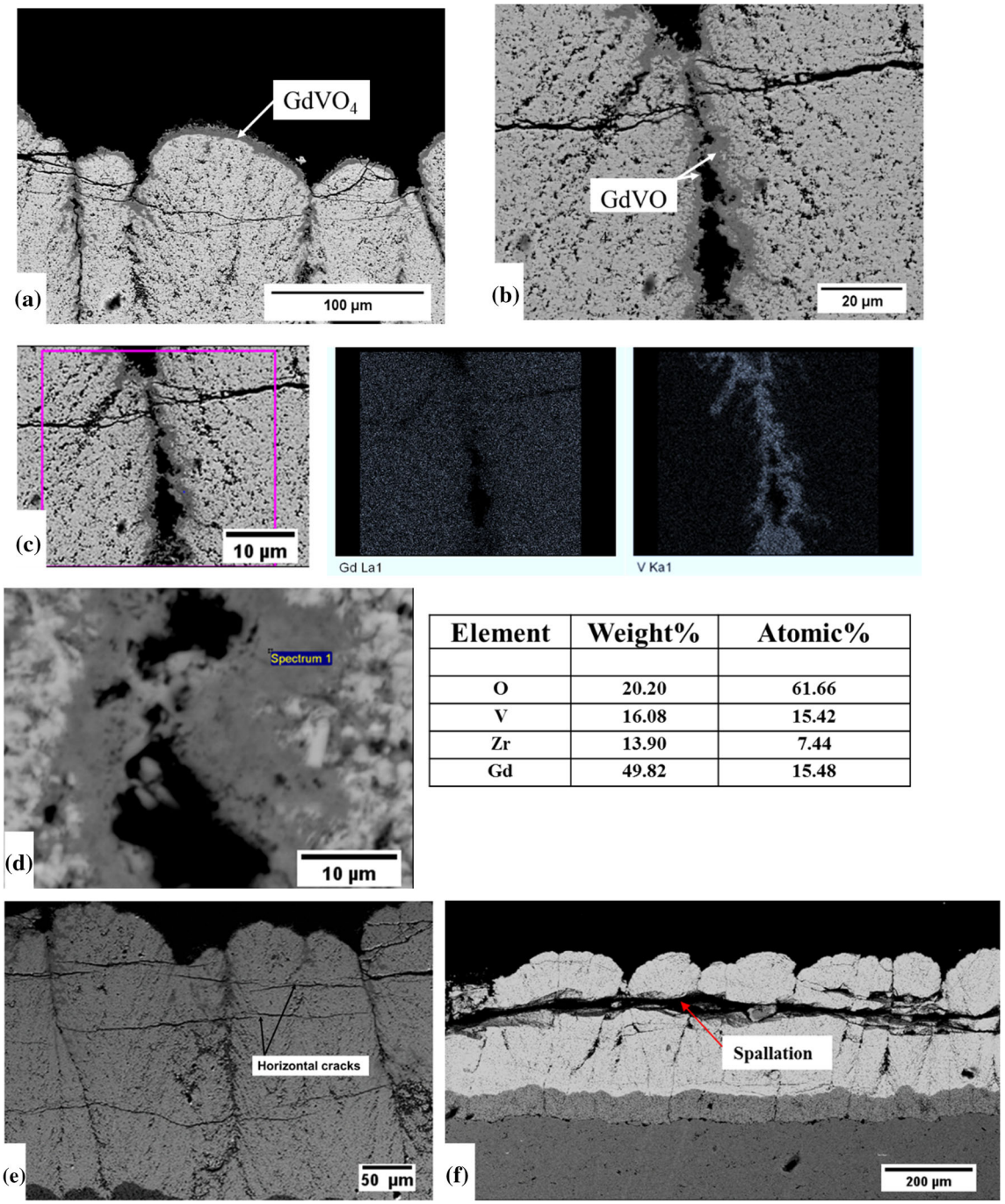

Element	Weight%	Atomic%
O	20.20	61.66
V	16.08	15.42
Zr	13.90	7.44
Gd	49.82	15.48

Fig. 8 Cross section of two-layer gadolinium zirconate coatings showing (a) $GdVO_4$ on the top surface, (b) $GdVO_4$ formation between the columns, (c) EDS map of $GdVO_4$ in between the columns, (d) Quantitative EDS measurement on the corroded layer, (e) horizontal cracks in the coating, and (f) spallation

formed, zirconia transforms to monoclinic. According to the work by Eichler et al. (Ref 21), the fracture toughness value of monoclinic zirconia is about 2 MPa $m^{1/2}$ which is reasonably close to that of YSZ. Thus the crack propagation in m-ZrO_2 could be as difficult as in the original YSZ. From the XRD results (Fig. 6a and b), the amount of monoclinic zirconia is higher in YSZ compared to GZ-based coatings (due to higher reactivity of the salts with YSZ). Due to the higher fracture toughness of m-ZrO_2 and YSZ, the cracks generated during the salt exposure could be difficult to propagate. In the case of GZ-based coatings, due to the lower amount of m-ZrO_2, the propagation of

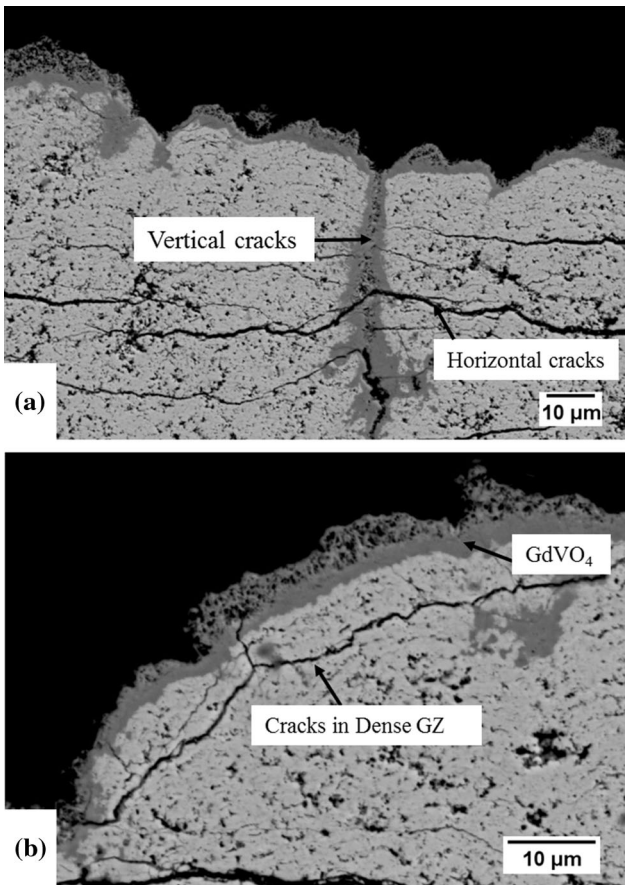

Fig. 9 Cracks in the three-layer system (a) in the second layer and (b) in the third layer

cracks occurs more in the gadolinium zirconate structure. With the lower fracture toughness of GZ, the crack propagation is, therefore, much faster. This in the combination of reduced strain tolerance is believed to have caused more severe coating damage during the corrosion tests conducted in this work. As a result, the slow reacting gadolinium zirconate is more susceptible to corrosion-induced damage than YSZ in coatings with columnar microstructures.

The three-layer coating system, with a relatively dense top layer which was initially thought to improve the corrosion resistance, did not show any improvement compared to the two-layer coating system. There are two reasons for this; First, there are vertical cracks in the coating, although fewer in number. These vertical cracks were difficult to avoid from a mechanical standpoint. The nominal thickness of the third layer is 30 μm, and it is deposited on the top of two layers having columnar structure and a combined thickness of 290 μm. During cooling, when the columns expand/contract in the first and the second layer, vertical cracks are also introduced in the third layer. Due to the presence of these vertical cracks, the damage is similar to the two-layer system. Furthermore, the deposited third layer was not totally dense, and the salts could still infiltrate and result in cracking within the third layer also.

It has to be noted that the above experiment causes accelerated corrosion in the coatings, and an actual turbine component may or may not encounter these harsh conditions. Nevertheless, the results of these tests can be used for qualitative ranking of different TBC materials. This test illustrates an important point that an improper combination of microstructure, and the coating material might result in more corrosion-induced damage though individually they may offer better resistance to corrosion. A proper combination of microstructure and the coating chemistry is, therefore, non-trivial when designing coatings that can perform against salt corrosion.

Conclusions

This study provides an insight on the corrosion mechanism and corrosion resistance of multi-layer gadolinium zirconate/YSZ and YSZ single-layer suspension plasma sprayed TBCs. When exposed to a mixture of vanadium pentoxide and sodium sulfate at 900 °C, multi-layer gadolinium zirconate-based coatings exhibited lower reactivity with the corrosive salts. The columnar microstructure of the coatings and low reactivity of the GZ allowed extensive salt penetration into the coating through the columnar gaps. The later formation of the corrosive product, $GdVO_4$, between the columns reduced the strain tolerance of the columnar microstructure and low fracture toughness of gadolinium zirconate allowed for extensive cracking within the coating. Furthermore, a relatively dense third layer on the top did not result in improvement of corrosion resistance as the damage occurred more in the second layer due to the salt infiltration through the vertical cracks in the coating.

The reference single-layer YSZ coating experienced less damage than the multi-layer coatings in part due to the corrosive species being immobilized in the upper portion of the coating. The corrosive products were formed inside the pores, unlike GZ where they were formed at the columnar gaps. The columnar structure of the YSZ coating, in combination with the superior fracture toughness of YSZ, allows it to; (a) tolerate greater stress before cracking and (b) reduce the rate of crack propagation in comparison with the GZ coatings.

A proposed solution to the infiltration of the multi-layer coatings in extremely harsh corrosion conditions would be to substitute the outer dense layer for a material that would be highly reactive with the corrosive salts; therefore, immobilizing them at the surface, preventing further penetration and damage. The focus of the further work is to understand the growth mechanism of corrosive products

and to improve the performance of the multi-layered systems based on the current understanding of their behavior under salt exposure.

Acknowledgments Vinnova in Sweden is gratefully acknowledged for the research funding.

References

1. N.P. Padture, M. Gell, and E.H. Jordan, Thermal Barrier Coatings for Gas-Turbine Engine Applications, *Science*, 2002, **296**(5566), p 280-284
2. B. Gleeson, Thermal Barrier Coatings for Aeroengine Applications, *J. Propuls. Power*, 2006, **22**(2), p 375-383
3. J.T. DeMasi-Marcin and D.K. Gupta, Protective Coatings in the Gas Turbine Engine, *Surf. Coatings Technol.*, 1994, **68-69**, p 1-9
4. M.J. Pomeroy, Coatings for Gas Turbine Materials and Long Term Stability Issues, *Mater. Des.*, 2005, p 223-231.
5. G.W. Goward, Progress in Coatings for Gas Turbine Airfoils, *Surf. Coatings Technol.*, 1998, **108-109**(1-3), p 73-79
6. S. Bose and S. Bose, Chapter 7–THERMAL BARRIER COATINGS (TBCs), *High Temperature Coatings*, 2007, p 155-232.
7. Z. Chen, S. Speakman, J. Howe, H. Wang, W. Porter, and R. Trice, Investigation of Reactions between Vanadium Oxide and Plasma-Sprayed Yttria-Stabilized Zirconia Coatings, *J. Eur. Ceram. Soc.*, 2009, **29**(8), p 1403-1411
8. M.H. Habibi, L. Wang, and S.M. Guo, Evolution of Hot Corrosion Resistance of YSZ, $Gd_2Zr_2O_7$, and $Gd_2Zr_2O_7$+YSZ Composite Thermal Barrier Coatings in Na_2SO_4+V_2O_5 at 1050 °C, *J. Eur. Ceram. Soc.*, 2012, **32**(8), p 1635-1642
9. D.R. Clarke and S.R. Phillpot, Thermal Barrier Coating Materials, *Materials Today*, 2005, p 22-29.
10. G. Mauer, M.O. Jarligo, D.E. Mack, and R. Vassen, Plasma-Sprayed Thermal Barrier Coatings: New Materials, Processing Issues, and Solutions, *J. Therm. Spray Technol.*, 2013, p 646-658.
11. R.M. Leckie, S. Krämer, M. Rühle, and C.G. Levi, Thermochemical Compatibility between Alumina and ZrO_2–$GdO_{3/2}$ Thermal Barrier Coatings, *Acta Mater.*, 2005, **53**(11), p 3281-3292
12. N. Curry, K. VanEvery, T. Snyder, and N. Markocsan, Thermal Conductivity Analysis and Lifetime Testing of Suspension Plasma-Sprayed Thermal Barrier Coatings, *Coatings*, 2014, **4**(3), p 630-650
13. N. Curry, K. VanEvery, T. Snyder, J. Susnjar, and S. Bjorklund, Performance Testing of Suspension Plasma Sprayed Thermal Barrier Coatings Produced with Varied Suspension Parameters, *Coatings*, 2015, **5**(3), p 338-356
14. S. Mahade, N. Curry, S. Björklund, N. Markocsan, and P. Nylén, Thermal Conductivity and Thermal Cyclic Fatigue of Multilayered $Gd_2Zr_2O_7$/YSZ Thermal Barrier Coatings Processed by Suspension Plasma Spray, *Surf. Coatings Technol.*, 2015, **283**, p 329-336
15. J. Wu, X. Wei, N.P. Padture, P.G. Klemens, M. Gell, E. Garciá, P. Miranzo, and M.I. Osendi, Low-Thermal-Conductivity Rare-Earth Zirconates for Potential Thermal-Barrier Coating Aplications, *J. Am. Ceram. Soc.*, 2002, **85**(12), p 3031-3035
16. Z.G. Liu, J.H. Ouyang, Y. Zhou, and S. Li, High-Temperature Hot Corrosion Behavior of Gadolinium Zirconate by Vanadium Pentoxide and Sodium Sulfate in Air, *J. Eur. Ceram. Soc.*, 2010, **30**(12), p 2707-2713
17. A.A. Abubakar, S.S. Akhtar, and A.F.M. Arif, Phase Field Modeling of V_2O_5 Hot Corrosion Kinetics in Thermal Barrier Coatings, *Comput. Mater. Sci.*, 2015, **99**, p 105-116
18. T.E. Strangman, Thermal Barrier Coatings for Turbine Airfoils, *Thin Solid Films*, 1985, **127**(1-2), p 93-106
19. G. Dwivedi, V. Viswanathan, S. Sampath, A. Shyam, and E. Lara-Curzio, Fracture Toughness of Plasma-Sprayed Thermal Barrier Ceramics: Influence of Processing, Microstructure, and Thermal Aging, *J. Am. Ceram. Soc.*, 2014, **97**(9), p 2736-2744
20. X. Zhong, H. Zhao, X. Zhou, C. Liu, L. Wang, F. Shao, K. Yang, S. Tao, and C. Ding, Thermal Shock Behavior of Toughened Gadolinium zirconate/YSZ Double-Ceramic-Layered Thermal Barrier Coating, *J. Alloys Compd.*, 2014, **593**, p 50-55
21. J. Eichler, U. Eisele, and J. Rödel, Mechanical Properties of Monoclinic Zirconia, *J. Am. Ceram. Soc.*, 2004, **87**(7), p 1401-1403